5-31-2019

Mercury Cycling in the North Pacific Subtropical Gyre as Revealed by Mercury Stable Isotope Ratios

Laura C. Motta

Joel D. Blum

Marcus W. Johnson

Blaire P. Umhau

Brian N. Popp

See next page for additional authors

Publication Info

Published in *Global Biogeochemical Cycles*, Volume 33, Issue 6, 2019, pages 777-794.

Global Biogeochemical Cycles

RESEARCH ARTICLE
10.1029/2018GB006057

Mercury Cycling in the North Pacific Subtropical Gyre as Revealed by Mercury Stable Isotope Ratios

Laura C. Motta[1], Joel D. Blum[1], Marcus W. Johnson[1], Blaire P. Umhau[2], Brian N. Popp[3], Spencer J. Washburn[1], Jeffrey C. Drazen[4], Claudia R. Benitez-Nelson[2], Cecelia C. S. Hannides[3], Hilary G. Close[5], and Carl H. Lamborg[6]

[1]Department of Earth and Environmental Sciences, University of Michigan, Ann Arbor, MI, USA, [2]School of Earth, Ocean and Environment, University of South Carolina, Columbia, SC, USA, [3]Department of Earth Sciences, University of Hawai'i at Mānoa, Honolulu, HI, USA, [4]Department of Oceanography, University of Hawai'i at Mānoa, Honolulu, HI, USA, [5]Rosenstiel School of Marine and Atmospheric Science, University of Miami, Miami, FL, USA, [6]Department of Ocean Sciences, University of California, Santa Cruz, CA, USA

Key Points:
- MMHg bioaccumulated in fish is derived primarily from Hg (II) deposited in atmospheric precipitation
- Marine particles host the majority of Hg available for production of MMHg in the open ocean
- Methylation and demethylation of Hg occurs throughout the euphotic and mesopelagic zones in the North Pacific Subtropical Gyre

Supporting Information:
- Supporting Information S1
- Data Set S1

Correspondence to:
L. C. Motta,
laumot@umich.edu

Citation:
Motta, L. C., Blum, J. D., Johnson, M. W., Umhau, B. P., Popp, B. N., Washburn, S. J., et al. (2019). Mercury cycling in the North Pacific Subtropical Gyre as revealed by mercury stable isotope ratios. *Global Biogeochemical Cycles*, *33*, 777–794. https://doi.org/10.1029/2018GB006057

Received 16 AUG 2018
Accepted 21 MAY 2019
Accepted article online 31 MAY 2019
Published online 26 JUN 2019

Abstract The oceans are an important global reservoir for mercury (Hg), and marine fish consumption is the dominant human exposure pathway for its toxic methylated form. A more thorough understanding of the global biogeochemical cycle of Hg requires additional information on the mechanisms that control Hg cycling in pelagic marine waters. In this study, Hg isotope ratios and total Hg concentrations are used to explore Hg biogeochemistry in oligotrophic marine environments north of Hawaii. We present the first measurements of the vertical water column distribution of Hg concentrations and the Hg isotopic composition in precipitation, marine particles, and zooplankton near Station ALOHA (22°45′N, 158°W). Our results reveal production and demethylation of methylmercury in both the euphotic (0–175 m) and mesopelagic zones (200–1,000 m). We document a strong relationship between Hg isotopic composition and depth in particles, zooplankton, and fish in the water column and diurnal variations in Δ^{199}Hg values in zooplankton sampled near the surface (25 m). Based on these observations and stable Hg isotope relationships in the marine food web, we suggest that the Hg found in large pelagic fish at Station ALOHA was originally deposited largely by precipitation, transformed into methyl-Hg, and bioaccumulated in situ in the water column. Our results highlight how Hg isotopic compositions reflect abiotic and biotic production and degradation of methyl-Hg throughout the water column and the importance of particles and zooplankton in the vertical transport of Hg.

1. Introduction

Mono-methylmercury (MMHg) is one of the most toxic forms of the global pollutant mercury (Hg) and is strongly retained at each trophic level in marine food webs, reaching high concentrations in piscivorous fish, the main source of exposure of MMHg to humans (Morel et al., 1998). Despite decades of research on Hg many details remain unclear about how, at what depths in the ocean, and in which marine environments Hg transforms to the neurotoxic MMHg form and bioaccumulates in marine organisms. The current understanding of the biogeochemical cycle of Hg suggests that Hg exists in several forms including Hg (II), gaseous elemental mercury (Hg(0)), and methylated Hg (MeHg), both as MMHg and dimethyl-Hg. The major forms of Hg in aquatic ecosystems are Hg (II) complexed to organic ligands, chloride or sulfide, and organic mercury in the form of MMHg (Fitzgerald et al., 2007; Morel et al., 1998). Within the marine water column, Hg transformations include not only methylation of Hg (II) by abiotic and biotic processes (Munson et al., 2018; Sunderland et al., 2009) but also degradation of MMHg to Hg (II) and Hg(0) by photochemical and dark biotic processes (Fitzgerald et al., 2007; Sunderland et al., 2009). The limited understanding of the marine cycle of Hg is in part because of technical challenges associated with tracking and measuring different chemical forms of Hg in marine environments, especially in organisms like plankton at the base of the food web.

Plankton communities are known to be an important link between marine particles and higher trophic level pelagic marine organisms (see Figure 1 and references therein). However, there have been few studies of Hg speciation (e.g., MMHg, Hg (II)) in zooplankton, phytoplankton, or marine particles (Gosnell & Mason, 2015; Hammerschmidt et al., 2013), or the chemical and biological pathways that control Hg speciation near

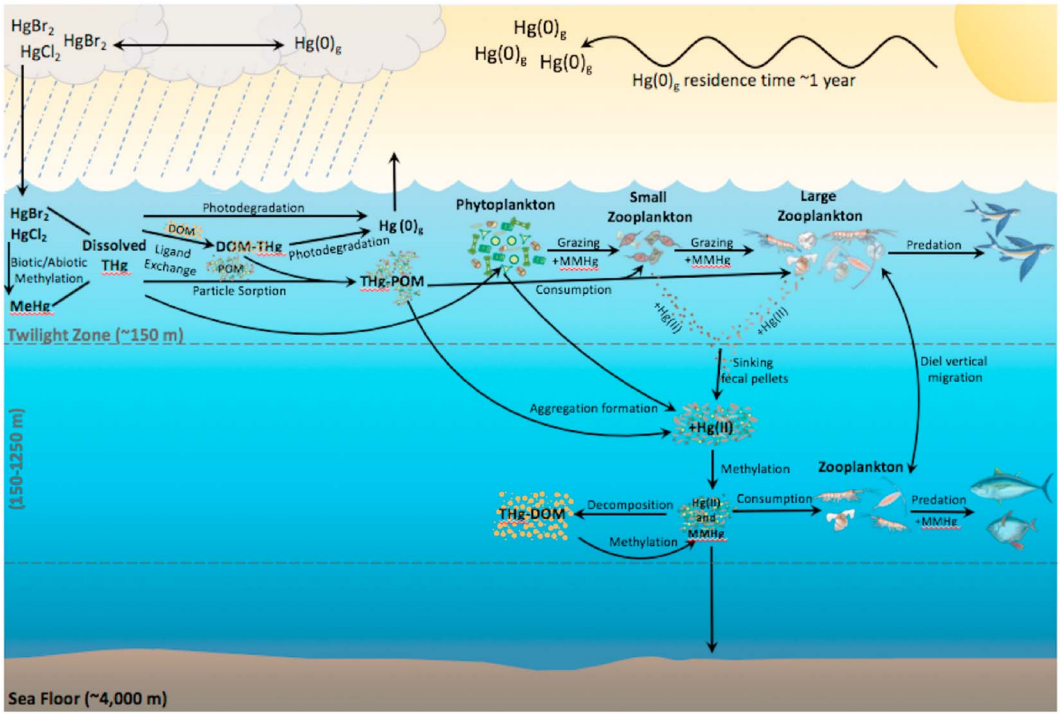

Figure 1. Biogeochemical cycle of Hg at Station ALOHA. The zooplankton and phytoplankton dynamics are explained in detail by Steinberg and Landry (2017). The zooplankton and phytoplankton interactions with Hg are explained in Mason et al. (1995, 1996), Watras and Bloom (1992), and Lee and Fisher (2016). Particle and zooplankton dynamics at Station ALOHA are explained in detail by Hannides et al. (2016), Umhau et al. (2016), and Close et al. (2014, 2015).

the base of the food web (Morel et al., 1998; Munson et al., 2015). Although dissolved total Hg (THg = Hg (II) + MeHg) concentrations have been reported in marine pelagic waters (Hammerschmidt & Bowman, 2012; Munson et al., 2015; Sunderland et al., 2009), details concerning the sources, transformations, and bioavailability of this Hg pool for uptake and bioaccumulation remain elusive. In the Pacific Ocean, elevated dissolved Hg concentrations are generally known to occur in oxygen deficient waters (Hammerschmidt & Bowman, 2012; Sunderland et al., 2009). Elevated oceanic Hg concentrations have been attributed to evasion from sediments (Hammerschmidt & Fitzgerald, 2006; Monperrus et al., 2003), emission from seafloor hydrothermal vents (Lamborg et al., 2006), and horizontal advection from coastal areas (Hammerschmidt & Bowman, 2012). Elevated MMHg in the water column has been attributed to biotic methylation of Hg (II) on marine particles (Blum et al., 2013; Cossa et al., 2011; Sunderland et al., 2009) and abiotic methylation in the water column (Munson et al., 2018). Thus, the biogeochemical pathway(s) for MMHg production in the open ocean are complex and remain uncertain.

Our study investigates the biogeochemical and photochemical pathways that control the distribution and speciation of Hg in the marine pelagic food web utilizing THg concentrations and Hg stable isotope ratios that vary following mass-dependent fractionation (MDF) and mass-independent fractionation (MIF). Hg isotope ratios have proven to be effective at tracking the sources and sinks of Hg in a number of estuarine and marine ecosystems (e.g., Kwon et al., 2015; Li et al., 2016; Senn et al., 2010; Štrok et al., 2015) and for exploring physicochemical reactions within the water column including reduction, photodegradation, oxidation, and methylation (e.g., Bergquist & Blum, 2007; Chandan et al., 2015; Kritee et al., 2009). Hg stable isotope ratios exhibit MDF (represented by δ^{202}Hg values) during all abiotic and biotic physicochemical reactions that have been investigated. In addition to MDF, Hg isotope ratios exhibit large-magnitude (≥0.4‰) MIF of odd-mass isotopes (odd-MIF; represented by Δ^{199}Hg and Δ^{201}Hg values) that has been attributed to photochemical transformations of Hg (Bergquist & Blum, 2007). Finally, MIF of even isotopes (even-MIF; represented by Δ^{200}Hg and Δ^{204}Hg values) is sometimes observed, particularly in rain and snow samples (e.g., Chen et al., 2012; Gratz et al., 2010), and it is strongly linked to atmospheric sources of Hg.

The objective of this study is to better understand the pathways of methylation and demethylation for the pool of Hg available for incorporation and bioaccumulation into marine food webs. To achieve this, we have analyzed Hg concentrations and stable isotope compositions of major components of the marine Hg cycle including precipitation, marine particles, zooplankton, and fish. We examine dissolved THg and MeHg concentrations, the relationship between the Hg isotopic composition of precipitation and surface marine particles, and Hg methylation in the water column, from the THg isotopic composition of marine particles and pelagic fish with depth. To assess Hg incorporation and bioaccumulation at the base of the food web, we examine THg concentrations and isotopic composition of marine zooplankton in three different size classes with depth. Finally, to investigate photochemical degradation of MMHg in surface waters we measure THg isotopic composition in zooplankton and pelagic fish.

The location of this study is Station ALOHA (22°45′N, 158°W), the site of the Hawaiian Ocean Time Series located in oligotrophic waters about 100 km north of the Hawaiian island of Oahu in the North Pacific Subtropical Gyre (NPSG). This station is characterized by little seasonal variability in salinity, temperature, or dissolved oxygen, resulting in a relatively stable thermocline and halocline (range 40–100 m) throughout the year. However, a rapid particle export pulse is typically observed from mid-July to mid-August and thus delivers bulk carbon (PC) and nitrogen at an increased rate to below the mixed layer (150 m) and into the deep ocean (4,000 m; Böttjer et al., 2017; Karl et al., 2012). Station ALOHA is near locations where previous work collected and analyzed pelagic fish for Hg concentrations and isotopic compositions (Blum et al., 2013; Choy et al., 2009).

2. Materials and Methods

Sample types analyzed in this study include rainfall collected on board the R/V *Kilo Moana* and on the Island of Hawaii, seawater from the surface to 1,000-m depth, small (1–53 μm) and large (>53 μm) marine particles sampled at depths ranging from 25 to 700 m, and marine zooplankton in five size classes (ranging from 0.2 to >5 mm) collected from the surface to 1,500-m depth. Marine samples were collected during three research cruises on board the R/V *Kilo Moana* at Station ALOHA (22.45°N, 158°W) in the NPSG in winter (KM 14-07, 19–28 February) of 2014, summer (KM 14-18, 29 August to 11 September) of 2014, and spring (KM 15-06, 2–11 May) of 2015. Measurements of water column dissolved oxygen and fluorescence were monitored during all sampling seasons using a Seabird SBE 9/11plus CTD deployed with two Sea-Bird SBE 3P temperature sensors, two Sea-Bird SBE 4C conductivity sensors, two Sea-Bird SBE 43 dissolved oxygen sensors, and a Wetlabs ECO FLNTU Chlorophyll Fluorometer and Turbidity sensor. All reagents used in the laboratory and at sea were trace metal grade unless otherwise noted.

2.1. Precipitation Collection and Analysis

Open ocean precipitation was collected during the summer season on an event basis using a manual collection method (Landis & Keeler, 1997). All of the Teflon and Pyrex glass components of the system were acid cleaned. The 1-L sample bottles were deployed with 20 mL of 1% (wt/v) HCl to prevent reduction of Hg (II). Collection funnels were uncovered only when it was raining and the ship was steaming into a head wind to reduce possible contamination from ship emissions. Due to infrequent precipitation, three separate rain events were combined into one sample to obtain sufficient Hg for isotope analysis. Additional samples were collected on land on the windward coast of the Island of Hawaii where trade winds bring moisture directly from the open ocean. These samples were collected at Hakalau Wildlife Refuge in December of 2005 (18 km from the coastline) on private property near the Waipio Valley lookout at the top of a cliff (300 m above the shoreline), and at the Nature Conservancy Ka'u Preserve (6 km inland from the ocean at shoreline level). Procedural field blanks were collected periodically during the sampling campaign using 1 L of deionized water.

All precipitation samples were further oxidized with 1% BrCl (wt/v), which was allowed to react with the water sample in dark, refrigerated storage for a minimum of 1 month. The oxidized precipitation samples were subsequently reduced, purged, and trapped into 1% $KMnO_4$ in 10% H_2SO_4 (wt/wt) solution for isotope analysis, following the procedure described by Washburn et al. (2017). Approximately 1 L of previously acidified and oxidized sample was weighed into an acid-clean 2-L borosilicate glass bottle and treated with 10 mL of 4.32 M NH_2OH-HCl to destroy free halogens, capped tightly, and allowed to react for a minimum of 30 min. Through one port of a three-port Teflon transfer cap, 100 mL of 10% $SnCl_2$ (wt/wt) in 20%

HCl (wt/wt) was delivered to the reaction bottle via a peristaltic pump, at a rate of ~3.3 mL/min. Another port delivered Hg-free air (Au-filtered) into the reactor via an internal sparger, while the final port was connected to a sparger inserted into a borosilicate glass trap containing between 5.5 and 6.5 g of 1% $KMnO_4$ trapping solution. Samples were purged for 3 hr while reactor contents were mixed vigorously using an acid-cleaned (10% wt/v HCl) Teflon stir bar. THg content of each sample bottle was determined by analyzing a small aliquot using cold vapor-atomic fluorescence spectrophotometry (CV-AFS; RA-3320FG+, Nippon Instruments). To determine Hg recovery, the THg concentration of small aliquots of each 1% $KMnO_4$ trapping solution was determined prior to transfer into a secondary trapping solution. The average purge and trap recoveries in precipitation samples was 93.7 ± 6.1% (1 SD [standard deviation], $n = 8$) and procedural blanks yielded between 22.7 and 39.4 pg of Hg ($n = 4$), representing less than 1.4% of Hg in sample trap solutions. Periodically, procedural blanks and procedural standards (NIST-UM-Almadén) were prepared and analyzed in tandem with precipitation samples.

2.2. Dissolved Hg and Particulate Hg Collection and Analysis

Seawater was collected for dissolved THg and MeHg analyses during the summer cruise using acid-cleaned (10% wt/v HCl) Go-Flo bottles deployed on an Amsteel line (Noble et al., 2012). THg dissolved concentrations were analyzed by dual Au-amalgamation cold vapor atomic fluorescence spectrometry (Tekran 2600), and dissolved MeHg concentrations were analyzed using ascorbic acid-assisted direct methylation (method adapted from Lamborg et al., 2012; Munson et al., 2015). Small (1–53 μm) and large (>53 μm) marine particles were sampled on all three cruises using in situ pumps (WTS-LV, standard, 8 L/min; McLane Research Laboratories, East Falmouth); water was passed sequentially through 53-μm pore-size nylon mesh and 1-μm pore-size quartz microfiber (QMA) filters with 142-mm diameter using a mini-MULVFS filter holder (Bishop et al., 2012). On the spring cruise, one pump was equipped with a pump head and motor with a maximum flow rate of 30 L/min, and high volume samples of particles >53 μm were collected. The large particles collected on the nylon mesh were sonicated and concentrated into a precombusted 47-mm QMA filter. The QMA filters of the small and large particles were digested using microwave assisted acid digestion, and aliquots of the digestions were measured for THg by CV-AFS (RA-3320FG+, Nippon Instruments). Details of the dissolved and particulate Hg analyses can be found in the supporting information (SI) Text S1.

In order to obtain enough Hg from small particles for isotope analysis, multiple 142-mm QMA filters were pooled from single depth horizons (±15 m). For samples from 25 m, two filters containing particles from ~4,000 L of filtered water were sufficient. In contrast, at all other depths (150, 400, and 690 m) larger numbers of filters representing particles from >6,500 L of filtered water were necessary (SI; Table S4a,b). Even more extensive pooling of material was required to obtain enough Hg from the >53 μm particles for a single isotope analysis. In the spring, a combined volume of ~ 35,000 L of water were filtered through 53 μm nylon mesh filters ($n = 10$ samples) at 30 L/min flow rates from 157 m. The combined nylon filters were rinsed onto three 47-mm diameter QMA filters (details in SI and references within). Following lyophilization, QMA filters from the same depth were processed together, and Hg was released from the particle matrix by two-stage combustion and trapping into an oxidizing solution (1% $KMnO_4$ in 10% H_2SO_4 (wt/wt); Biswas et al., 2008). A small aliquot of the trap solution was measured for THg concentration by CV-AFS (RA-3320FG+, Nippon Instruments). Combustion performance was monitored with procedural blanks, microfiber quartz filter blanks and combustion blanks (Table S4a,b).

For stable isotope ratio measurements of Hg the initial $KMnO_4$ trap solutions were chemically reduced with NH_2OH-HCl and $SnCl_2$ and Hg(0) was purged into smaller secondary traps containing 6 g of 1% $KMnO_4$ (wt/v) prepared in 10% H_2SO_4 (v/v) for additional purification and preconcentration.

2.3. Zooplankton Collection and Analysis

Zooplankton were collected in summer and spring at Station ALOHA using a 1-m^2 Multiple Opening/Closing Net and Environmental Sensing System (Wiebe et al., 1985) equipped with nine sampling nets. Most of the zooplankton were collected in summer during the day ($n = 2$ tows) and night ($n = 3$ tows). Each tow collected material from nine depth intervals spanning the ocean surface to 1,500 m (0–50, 50–100, 100–150, 150–200, 200–300, 300–500, 500–700, 700–1,000, and 1,000–1,500 m). In spring, four separate net tows were conducted to collect additional samples from a single depth interval (500–700 m). This was

done to provide enough sample material to assess variability in Hg content and isotopic composition in a pool of material well constrained in terms of depth, areal extent, and time. Following collection, the cod ends of each net were retrieved and immediately immersed in chilled surface seawater. Zooplankton samples collected in the cod ends were wet sieved into five separate size fractions using stacked 0.2-, 0.5-, 1.0-, 2.0-, and 5.0-mm mesh sieves, and the separated size fractions were filtered onto acid-cleaned, preweighed 47-mm diameter 0.2-mm synthetic nylon mesh filters. To make sure that the dominant species were zooplankton, our smallest sieve was 0.2 mm, which in the oligotrophic gyre excludes nearly all phytoplankton species (Pasulka et al., 2013). Briefly, the dominant zooplankton in the 0.2- to 1-mm size fractions were copepods and ostracods, and the 5-mm size fraction included euphaeids, amphipods, and chaetognaths. All samples were lyophilized and then homogenized using an acid cleaned agate mortar and pestle (Hannides et al., 2016).

For THg determination about 10 mg of zooplankton from each tow and size fraction was digested in reverse aqua regia (0.1 mL HCl:0.3 ml HNO_3; Optima, Fisher Scientific) overnight. Digest solutions were brought to a final volume of 4 mL with sequential additions of BrCl, H_2O_2 (Suprapur; MilliporeSigma, VWR Scientific), and deionized water. Multiple preparations of acid matrix blanks, combustion blanks, and certified reference material (TORT-2, National Research Council Canada) were analyzed for quality control.

For zooplankton, limited availability of bulk material necessitated pooling of samples for measurement of THg stable isotopic compositions, especially from depths below the euphotic zone (> 175 m; Table S2). Within each of six target depth intervals (Table S2) four zooplankton size fractions were combined to produce samples representing small (0.2–1 mm) and intermediate (1–5 mm) size zooplankton. The fifth and largest size class (>5 mm), which included occasional small fish as well as large zooplankton, was analyzed separately. All samples measured for Hg isotope ratios included material from more than one tow. For the three depth intervals at 500 m and above (e.g., 0–50, 100–150, and 300–500 m) day and night samples of the small, intermediate, and large size classes were measured separately for Hg isotope ratios. For the three depth intervals below 500 m (500–700, 700–1,000, and 1,000–1,500 m) separate day and night results could be obtained only for the intermediate and large size classes. Results for the small size class from the three depth intervals below 500 m include material combined from both day and night tows. Zooplankton samples were placed in ceramic boats in a two-stage combustion furnace, combusted similarly to the large and small particle QMA filters, and trapped in a 1% $KMnO_4$ solution for isotope analysis.

2.4. Fish Collection and Analysis

Twelve individual fish samples were analyzed for THg, from which 10 THg isotopic measurements were obtained. Three different individuals of the *Lampris* sp. were combined to obtain enough Hg for isotope analysis; details can be found in the SI tables (Table S1a). Lyophilized fish samples were combusted similarly to the particles and zooplankton and trapped in a 1% $KMnO_4$ solution for isotope analysis.

2.5. Hg Isotope Analysis

Each combusted sample trapped in 1% $KMnO_4$ solution was purged into a secondary 1% $KMnO_4$ trapping solution to remove matrix interferences from combustion residues and to concentrate THg for isotopic analysis (Blum & Johnson, 2017). All samples were preconcentrated in a 1% $KMnO_4$ solution and analyzed for Hg stable isotope compositions using a multiple collector inductively coupled plasma mass spectrometer (Nu Instruments) with a continuous flow cold vapor generation inlet system with $SnCl_2$ reduction (Blum & Bergquist, 2007; Lauretta et al., 2001). Prior to isotope analysis, the Hg concentrations of the 1% $KMnO_4$ sample trap solutions were matched to the bracketing standards (SRM NIST 3133) for each of the mass spectrometry sessions. The THg concentrations of the 1% $KMnO_4$ sample trap solutions for all samples are provided in Tables S1a–e.

MDF of Hg isotopes is reported as δ^{202}Hg values in permil (‰) relative to NIST SRM 3133 (equation (1)). MIF of Hg isotopes is calculated as the difference between the measured δ^{202}Hg value and that which would be predicted based on mass dependence for a given isotope. It is reported as Δ^{xxx}Hg in ‰ (equation (2)), where xxx is the mass of each Hg isotope, that is, 199, 200, 201, and 204, and β is the mass proportionality constant (0.2520, 0.5024, 0.7520, and 1.493, respectively; Blum & Bergquist, 2007).

$$\delta^{xxx}\mathrm{Hg}\ (‰) = \left(\left[\left(^{202}\mathrm{Hg}/^{198}\mathrm{Hg}\right)_{\mathrm{unknown}}/\left(^{202}\mathrm{Hg}/^{198}\mathrm{Hg}\right)_{\mathrm{SRM3133}}\right]-1\right)\times 1000 \quad (1)$$

$$\Delta^{xxx}\mathrm{Hg} = \delta^{xxx}\mathrm{Hg} - \left(\delta^{202}\mathrm{Hg}\times\beta\right) \quad (2)$$

Procedural process blanks and standard reference materials (TORT-2 and DORM-3 for combusted samples, and UM-Almadén for purge and trap samples) were processed alongside samples in an identical manner (Table S1a–f). Process yields from secondary purge and trapping of the 1% $KMnO_4$ trap solutions averaged 97% ± 8% (1 SD, minimum = 85.5%). The long-term analytical uncertainty of Hg isotopic composition of the samples, most of which could be measured only once, was estimated as ±2 SD based on repeated measurements across runs of the appropriate standard reference materials (UM-Almadén, DORM-3, ERM-CE464, NIST-CRM1947, and TORT-2; Table S1b). When comparing specific samples with each other or a population of samples, ±1 SD is reported (Blum & Bergquist, 2007). For data analysis the majority of statistical tests were completed using the Wilcoxon test (unless otherwise noted) because the sample size was usually too small for a *t* test. Linear regressions were completed using the York regression, which considers errors in both the *X* and *Y* axes (York, 1969).

3. Results

For all seasons the oxygen minimum was located at ~700 m and dissolved oxygen ranged from 25 to 34 μmol/kg. Fluorescence was lowest in February and highest in September, and the deep chlorophyll maximum was at ~125 m for all seasons (0.4–0.9 mg/m^3). The mixed layer depth was ~100 m for the winter and ~45 m for the spring and summer.

Vertical profiles of dissolved THg and MeHg measured at Station ALOHA during the summer are similar to results previously published by Munson et al. (2015) at 17°N, 154°W and Sunderland et al. (2009) at 23°N, 152°W and ranged from 0.07 to 0.43 ng/L for THg and 5.0×10^{-3} to 2.5×10^{-2} ng/L for MeHg (Figure S1). Small particles (1–53 μm) collected at Station ALOHA had the highest THg at the surface and declined with depth reaching an average of $4.57 \times 10^{-3} \pm 7.5 \times 10^{-4}$ ng/L (1 SD, $n = 5$;S2). Large particles were orders of magnitude lower in THg than the smaller fraction at the same depths (150 m) and ranged from 1.70×10^{-4} ng/L in September to 6.66×10^{-4} ng/L in May (Figure S2). Additional details regarding the vertical profiles are found in the SI, and all mercury isotope data and THg concentrations are presented in SI Tables S1–S4.

3.1. Precipitation

The average THg of samples collected on the Island of Hawaii was 11.8 ± 7.5 ng/L ($n = 8$, 1 SD). For these land-based samples, the average isotopic values are $\delta^{202}\mathrm{Hg} = 0.07 \pm 0.08‰$, $\Delta^{199}\mathrm{Hg} = 0.33 \pm 0.24‰$, and $\Delta^{200}\mathrm{Hg} = 0.14 \pm 0.05‰$ ($n = 7$; 1 SD). The THg concentration of open ocean precipitation (9.6 ± 2.6 ng/L; 1 SD, $n = 2$) was within uncertainty of the land-based samples. The Hg stable isotope composition of the single open ocean precipitation sample was $\delta^{202}\mathrm{Hg} = 0.15‰$, $\Delta^{199}\mathrm{Hg} = -0.02‰$, and $\Delta^{200}\mathrm{Hg} = 0.08‰$. This is within uncertainty of the average $\delta^{202}\mathrm{Hg}$ and $\Delta^{200}\mathrm{Hg}$ values determined for precipitation from the Island of Hawaii. The $\Delta^{199}\mathrm{Hg}$ value was slightly more negative; however, limited sampling does not allow for a general conclusion that open ocean precipitation has more negative $\Delta^{199}\mathrm{Hg}$ than precipitation collected on land. The lack of distinction in isotopic composition between open ocean and land-based precipitation is supported by the observation that $\Delta^{201}\mathrm{Hg}$ values from the samples collected on the island of Hawaii ($\Delta^{201}\mathrm{Hg} = 0.32 \pm 0.23‰$, 1 SD, $n = 7$) overlap with the single open ocean sample within analytical uncertainty ($\Delta^{201}\mathrm{Hg} = 0.10‰$).

3.2. THg Isotopic Composition of Marine Particles

At the shallowest depth of 25 m, $\delta^{202}\mathrm{Hg}$ values for small particles were on average $-0.10 \pm 0.01‰$ (1 SD, $n = 3$; Figure 2a and Table S1c), and there were no seasonal differences. At 150 m, values were statistically lower than at all other depths (−0.27 to −0.14‰, $n = 4$, 1 SD = 0.06‰, average = −0.20‰), and there was no statistically significant seasonal variation at this depth (Wilcoxon test, $W = 33$, $p < 0.01$). At 400 m, values ranged from $\delta^{202}\mathrm{Hg} = -0.22‰$ in February to $\delta^{202}\mathrm{Hg} = 0.08‰$ in May. There was no sample collected in September. The February value from 400 m is statistically identical to the average

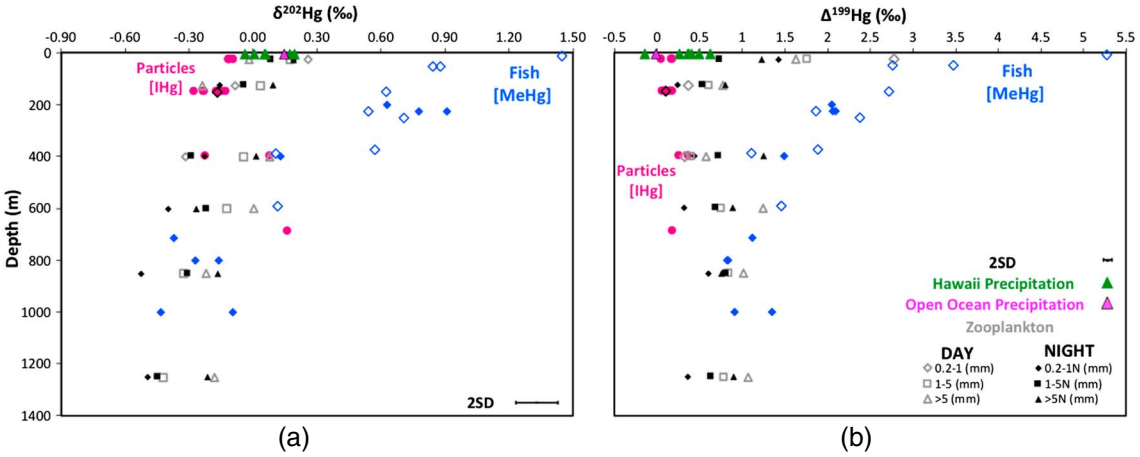

Figure 2. (a) δ^{202}Hg and (b) Δ^{199}Hg values of samples as a function of depth in meters. Green triangles are precipitation samples collected on the island of Hawaii, and the pink triangle is a shipboard precipitation sample. The magenta circles are small particles, and the diamonds are large particles. The open blue diamonds are pelagic fish from the North Pacific Subtropical Gyre near Hawaii published by Blum et al. (2013), and the filled blue diamonds are additional samples from Station ALOHA. The open gray symbols are zooplankton collected during the day, and the filled black symbols are zooplankton collected during the night. Measurement uncertainty Almaden Δ^{199}Hg ± 0.05 and TORT-2 δ^{202}Hg ± 0.10, 2 SD).

at 150 m (Wilcoxon test, $W = 18$, $p < 0.03$), while the September value from 400 m has a similar value to the single sample analyzed from May at 690 m (δ^{202}Hg = 0.17 ‰).

The Δ^{199}Hg values in the small particles were relatively constant in the upper 150 m across seasons (Figure 2b, 0.06 to 0.18‰, average = 0.12 ± 0.05‰, 1 SD, $n = 7$) and the standard deviation of the average value was equal to the measurement uncertainty (Almaden, 2 SD Δ^{199}Hg ± 0.10). The deeper samples from all seasons, collected from 400 and 690 m, had significantly higher Δ^{199}Hg values than those from the upper 150 m (25–150 m average = 0.12‰; 400–690 m average = 0.27‰, Wilcoxon test, $W = 23$, $p < 0.03$). The δ^{202}Hg and Δ^{199}Hg values for the large particles (>53 μm) collected in May at 150 m are nearly the same as for the small particles collected in the same season at the same depth (δ^{202}Hg = −0.17‰ and Δ^{199}Hg = 0.11‰). The Δ^{200}Hg values for all the particles were nearly the same throughout the water column (Figure S3, Δ^{200}Hg = 0.05 ± 0.05‰, 1 SD, $n = 12$)

3.3. Zooplankton

In the upper 125 m, THg concentrations in zooplankton are highest for the smallest size class by an average of 7.5 ng/g relative to the larger size classes (0.5–1, 1–2, and >5 mm, Wilcoxon test, $W = 127$, $p < 0.01$), and THg increases with depth to 500–700 m for all size classes (Figure 3 and Table S3). Below 700 m, THg within the smallest size class decreases with depth, while in the larger size classes (2 to >5 mm) THg increases with depth. There were significant THg diurnal variations within the mesopelagic (200 to 1,500 m); zooplankton collected at night had significantly higher THg concentrations than samples collected during the day (Figure 3; day-night paired, Wilcoxon test, $W = 137$, $p < 0.01$). To examine the effects of zooplankton diel migration on mobilization of Hg within the water column, we normalized zooplankton Hg content to the volume of seawater filtered by each net (in units of nanograms Hg per liter of seawater; Figure 3b). The Hg per liter depth profiles of the zooplankton follow the same trend as for summer 2014 migrant zooplankton biomass (Hannides et al., 2016).

The Hg isotope composition of zooplankton clearly differs between size classes and between depth of collection over the six target mean depth intervals (0–50, 100–150, 300–500, 500–700, 700–1,000, and 1,000–1,500 m; see Figures 2, S4a, and S4ab and Table S1d). The δ^{202}Hg values decline with depth for all the size classes, and there was no statistical difference in the rate of decline of δ^{202}Hg values with depth between the size classes (Figure S4a, average slope δ^{202}Hg/Km = −0.42 ± 0.06, $n = 4$, 1 SD, $p < 0.02$), with the exception of the >5-mm size fraction, where there was no relationship with depth for the samples collected during the day (Wilcoxon test, $W = 15$, $p = 0.05$). At each depth the range of δ^{202}Hg values across the different size classes is ~0.35‰. In surface waters both small and large size classes, respectively, have the highest (0.26‰)

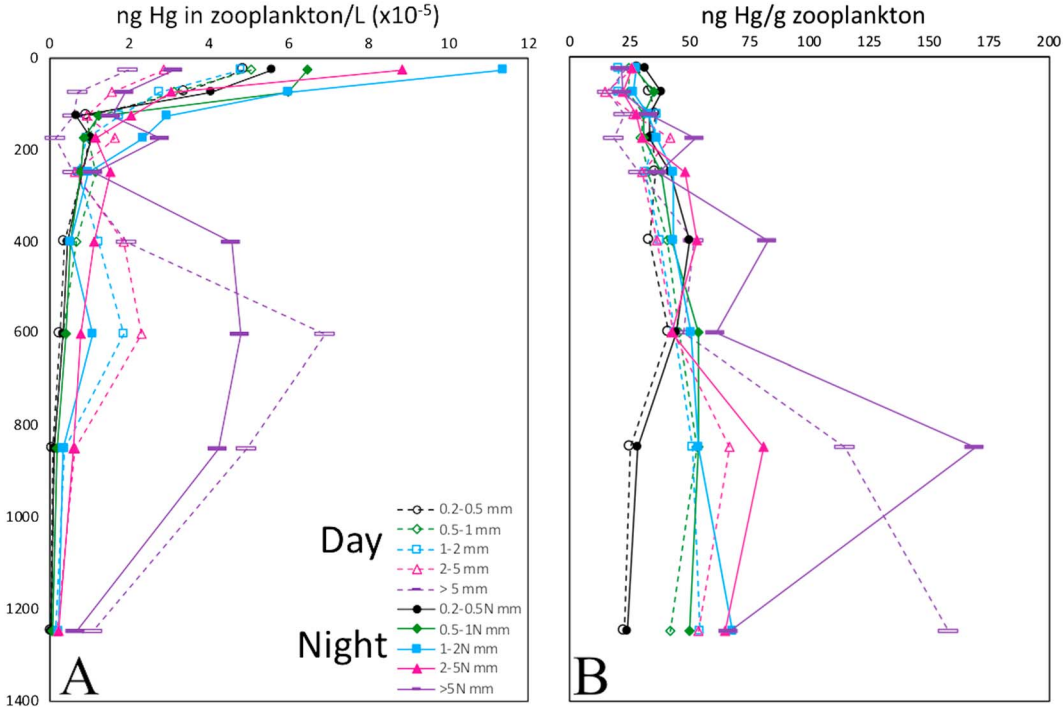

Figure 3. Vertical profiles of total Hg recovered from zooplankton biomass sampled during day (open symbols) and night (closed symbols). (a) normalized to zooplankton dry weight and (b) normalized to total water volume sampled by Multiple Opening/Closing Net and Environmental Sensing System tows.

and lowest (−0.02‰) δ^{202}Hg values. At greater depths (100 to 1,500 m) δ^{202}Hg values are lowest for the small size class (δ^{202}Hg average = −0.31 ± 0.15‰), higher for the intermediate size class (δ^{202}Hg average = −0.22 ± 0.16‰), and highest for the >5-mm size class (δ^{202}Hg average = −0.11 ± 0.13‰).

In contrast to δ^{202}Hg values, surface water Δ^{199}Hg values varied more broadly, differing by 2‰ across size classes. The smallest size fraction had the highest Δ^{199}Hg values, and the samples collected during the day had higher Δ^{199}Hg values than those collected at night (Figures 2b and S4b and Table S1d). Samples from greater depths (125–1,250 m) had statistically lower Δ^{199}Hg values than those from the surface (Wilcoxon test, $W = 15$, $p < 0.02$) and had smaller ranges in Δ^{199}Hg. Unlike δ^{202}Hg values, there were no significant changes in Δ^{199}Hg values below 125 m (100–1,500 m, average slope, Δ^{199}Hg/Km = −0.04, $n = 27$), and there was no diurnal signature (Wilcoxon test, $W = 40.5$, $p > 0.1$).

Zooplankton samples did not have a significant trend in Δ^{200}Hg with depth, and averaged 0.07 ± 0.08‰ (1 SD, $n = 33$). There was a small diurnal contrast in Δ^{200}Hg values obtained from the shallowest samples and from samples collected at 400 m (Figure S3). However, there was no diurnal contrast in Δ^{204}Hg values (which is also produced by even-MIF), suggesting that the negative values for Δ^{200}Hg at 400 m are likely due to an analytical artifact. Δ^{204}Hg values are typically inversely correlated with Δ^{200}Hg values (Blum & Johnson, 2017; Demers et al., 2013), and, therefore, negative Δ^{200}Hg and Δ^{204}Hg values are very rare (Blum et al., 2014). In addition, the magnitude of even-MIF is small relative to the measurement uncertainty for standard reference material TORT-2 (Δ^{200}Hg ± 0.09‰ and Δ^{204}Hg ± 0.13‰; 2 SD, $n = 31$).

Replicate collections of material from a single depth range were obtained to determine the variability in zooplankton Hg isotopic composition (Table S1e; 500–700 m). For the intermediate fraction, the variability associated with average δ^{202}Hg, Δ^{199}Hg, and Δ^{200}Hg values was 0.05‰, 0.07‰, and 0.06‰ (1 SD), respectively. For the large fraction the 1 SD of average δ^{202}Hg, Δ^{199}Hg, and Δ^{200}Hg values was 0.14‰, 0.2‰, and 0.04‰, respectively. Limited availability of <1-mm zooplankton material prevented determination of external reproducibility for the small size class fraction. Instead, two single analyses were performed on <1-mm zooplankton material pooled from all four nets but separated into <0.5- and 0.5- to 1-mm subfractions. Small differences between these two subfractions for δ^{202}Hg (0.04‰), Δ^{199}Hg (0.11‰), and Δ^{200}Hg

(0.02‰) suggests that within-class variability in the small size class (0.2–1 mm) is comparable to, or smaller than, that of the intermediate size class (1–5 mm).

3.4. Pelagic Fish

Dry-mass THg concentrations in fish range from less than 100 to more than 2,000 ng/g. In the large pelagic species (*Lampris* sp. and *Thunnus obesus*) THg concentrations were a factor of 10 to 100 higher than THg concentrations in zooplankton from comparable depths. Small micronekton that feed in upper mesopelagic waters (~400 m, *Idiacanthus fasciola*) had average THg content less than a factor of 2 higher than zooplankton from comparable depths. However, deeper-feeding micronekton (700 to >1,000 m, *Anoplogaster cornuta*, *Cyclothone pallida*, and *Melanocetus johnsonii*) had THg content almost an order of magnitude higher than zooplankton from similar depths. Estimates of external variability associated with fish isotope results is hampered by the small number of individuals sampled per species. However, the results obtained from multiple individuals and the averages of 1 SD uncertainties associated with species replicate δ^{202}Hg, Δ^{199}Hg, and Δ^{200}Hg values are 0.12‰, 0.13‰, and 0.03‰, respectively (Table S1e). δ^{202}Hg and Δ^{199}Hg values in Figures 2a and 2b illustrate that for the pelagic fish, δ^{202}Hg and Δ^{199}Hg values decline with depth. In contrast, there were no statistically significant differences with depth in Δ^{200}Hg values, which averaged 0.09 ± 0.04‰. A single sample of *Idiacanthus fasciola* at 400 m had an anomalous Δ^{200}Hg value of −0.16‰, which may be an analytical artifact. The pelagic fish samples with a depth of occurrence between 225 and 400 m had a similar Hg isotopic composition to fish samples from the NPSG at similar depths. Fish from greater depths (700–1,000 m) also follow the same trend reported by Blum et al. (2013).

4. Discussion

Here we integrate measurements of the stable isotopic composition of Hg in components of the marine biogeochemical cycle in order to address some of the outstanding questions in marine Hg biogeochemistry. Our main focus is on understanding Hg dynamics in the pelagic food web, abiotic and biotic production and degradation of MMHg throughout the water column, and the importance of particles and zooplankton to the marine biogeochemical cycle of Hg. We report that in the NPSG, at the base of the marine food web, the fraction of THg associated with marine particles or zooplankton per liter of water is very small relative to dissolved THg. For example, between 150–175 m dissolved THg (0.15 Hg ng/L) accounts for 96% of THg and is 5 orders of magnitude greater than zooplankton (0.2- > 5 mm; $1.24 \times 10^{-5} \pm 0.50 \times 10^{-5}$ ng/L, 1 SD, $n = 16$), 3 orders of magnitude greater than small particles (1–53 μm; $6.46 \times 10^{-3} \pm 1.84 \times 10^{-3}$ Hg ng/L, $n = 3$), and about 4 orders of magnitude greater than large particles (>53 μm; 4.18×10^{-4} Hg ng/L, $n = 2$). To guide our discussion, we provide a graphic that displays our conceptual model of the marine Hg cycle (Figure 1).

4.1. Dissolved THg and MeHg Vertical Profiles

The vertical profiles of dissolved THg and MeHg (MMHg+dimethyl-Hg) that we measured at Station ALOHA are similar to those of other North Pacific Ocean profiles (Hammerschmidt & Bowman, 2012; Laurier et al., 2004; Munson et al., 2015; Sunderland et al., 2009). In our study, surface water MeHg was within the range of values reported by Sunderland et al. (2009) at 23°N, 155°W but was somewhat greater than the values reported by Munson et al. (2015) at 17°N, 155°W. This variability in surface ocean MeHg concentrations is likely the result of spatial variation in MeHg production and degradation rates as well as differences in partitioning of dissolved MeHg between water and particle surfaces due to seasonal changes in productivity (Laurier et al., 2004; Sunderland et al., 2009). Vertical profiles of dissolved Hg in the NPSG have been well characterized in previous work (Hammerschmidt & Bowman, 2012; Laurier et al., 2004; Munson et al., 2015; Sunderland et al., 2009) and will not be discussed further here. Details of the dissolved Hg speciation at Station ALOHA are found in the SI and references therein (SI Text S2)

4.2. Hg Isotope Ratios as Indicators of Hg Transformation in the NPSG

4.2.1. Hg Isotope Ratios in Surface Waters (Upper 25 m)

As a starting point for the interpretation of the Hg isotope ratios in our study we assume that a significant portion of the Hg available for bioaccumulation in the water column was originally derived from precipitation, as this is considered to be the major source of Hg to the surface ocean (Figure 1; Fitzgerald et al., 2007; Mason & Sheu, 2002; Sunderland et al., 2009). It is challenging to fully link the Hg isotopic composition of

precipitation to that of Hg entry to the food web, because 50–70% of Hg in precipitation is potentially emitted back to the atmosphere (Andersson et al., 2011; Strode et al., 2007). The remaining dissolved Hg may undergo further transformation, including methylation, particle sorption, or additional photochemical reduction. There is also limited understanding of photochemical degradation of Hg (II), the potential uptake of gaseous Hg(0) in surface marine waters, and the impact of associated isotopic fractionation on the Hg isotopic composition of the dissolved Hg pool. This is because in ocean water the fraction of Hg complexed to organic ligands may not be the dominant form of THg (Lamborg et al., 2003), and it has been demonstrated that Hg stable isotope signatures associated with Hg (II) photoreduction depends on the complexing ligand (Zheng & Hintelmann, 2010). It is also difficult to evaluate the role of evasion and uptake of Hg(0) because a portion of Hg(0) may be reoxidized in the marine boundary layer (Hedgecock & Pirrone, 2001; Laurier et al., 2004; Sprovieri et al., 2010) or redeposited to the ocean in precipitation. Finally, direct measurements of Hg isotopic composition in the dissolved pool of THg are difficult due to the low THg concentrations in pelagic waters and the challenge associated with concentrating sufficient quantities of dissolved Hg for analysis. The Hg isotopic composition of seawater has been measured in only one study, in a costal location (Štrok et al., 2015). The Δ^{199}Hg values for dissolved THg from Arctic coastal waters (Δ^{199}Hg average = 0.22 ± 0.06‰, 1 SD) are within the range of values measured for marine particles in the NPSG. In contrast, the δ^{202}Hg values of the dissolved THg in the Arctic are considerably more negative (δ^{202}Hg average = −2.08 ± 0.61‰, 1 SD) than particles in the NPSG. This is not surprising because the Canadian Artic Archipelago has Hg inputs not only from precipitation but also from riverine discharge (Fisher et al., 2012; Sunderland & Mason, 2007; Cossa et al., 2018).

Measurements of the Hg isotopic composition of precipitation and marine particles allow a reasonable estimation of the Hg isotopic composition of the bioavailable Hg pool. In surface waters, Hg enters the food web when phytoplankton incorporate dissolved THg from passive uptake or when zooplankton graze on marine particles or phytoplankton. This results in Δ^{200}Hg and Δ^{204}Hg values in surface zooplankton that retain a positive Δ^{200}Hg and negative Δ^{204}Hg signature of Hg from precipitation (zooplankton: Δ^{200}Hg = 0.11 ± 0.09‰ and Δ^{204}Hg = −0.07 ± 0.08‰, 1 SD, n = 6; precipitation: Δ^{200}Hg = 0.13 ± 0.05‰ and Δ^{204}Hg = −0.26 ± 0.17‰, n = 8; Figure S3). The THg isotopic composition of marine particles in surface waters likely represent the THg isotopic composition that is exported to the ocean interior. Below the mixed layer particulate organic matter (POM) is the primary pathway by which Hg is transported to depth in the ocean and is the source of Hg that is available to enter the pelagic food web (Figure 1; Lamborg et al., 2016; Sunderland et al., 2009; Zaferani et al., 2018). This is because metazoans rely on marine particles as food resources, and dissolved Hg would have to be either sorbed to particles or assimilated by phytoplankton in order to be transferred higher in the food web as illustrated in Figure 1.

The size classes of particles we collected contain both phytoplankton biomass and other particles, such as marine snow and detritus, and both small and large particles have been identified as food sources for zooplankton and micronekton at Station ALOHA (Choy et al., 2015; Gloeckler et al., 2018; Hannides et al., 2016). The δ^{202}Hg values show a small negative offset (0.18‰) between precipitation (n = 8) and small particles (n = 3; Figures 2a and 2b); this offset is consistent with the MDF of Hg that occurs during binding to thiol functional groups associated with organic matter and sorption to particles (Jiskra et al., 2012; Wiederhold et al., 2010). The 0.18‰ offset in δ^{202}Hg is small compared to the offset observed in experimental sorption studies (Jiskra et al., 2012; Wiederhold et al., 2010), but this is not surprising because experiments used pure goethite or thiol ligands, and Hg sorption experiments do not take into consideration the effects of the high ionic strength of seawater. Although the Δ^{199}Hg and Δ^{200}Hg values of precipitation overlap with those of the particles, the range of Δ^{199}Hg and Δ^{200}Hg values in particles is narrow suggesting that isotopic variability attributed to individual precipitation events may be homogenized in the surface ocean as Hg undergoes exchange with particles.

4.2.2. Hg Stable Isotope Ratios in the Lower Epipelagic and Upper Mesopelagic (150- to 700-m Depth)

Below the mixed layer even-MIF values support the idea that the main source of Hg to the marine food web is particulate Hg. The even-MIF isotopic composition of the particles is nearly the same throughout the water column and is similar to the surface water particulate matter isotopic signature (average, Δ^{200}Hg = 0.06 ± 0.03‰ and Δ^{204}Hg = −0.10 ± 0.06‰, n = 9; 1 SD). The zooplankton have a very narrow range of even-MIF values below the mixed layer (Δ^{200}Hg = 0.06 ± 0.07‰ and Δ^{204}Hg = −0.06 ± 0.07‰, n = 9; 1 SD) compared to precipitation, and the zooplankton overlap with the Δ^{200}Hg and Δ^{204}Hg values of the

particles. This is because below the mixed layer metazoans primarily consume POM (Hannides et al., 2016). As a consequence, the average even-MIF of pelagic fish in NPSG ($\Delta^{200}Hg = 0.07 \pm 0.05‰$ and $\Delta^{204}Hg = -0.11 \pm 0.06‰$, $n = 9$; 1 SD) is also similar to the particles and zooplankton.

The THg $\delta^{202}Hg$ values of the particles below the mixed layer also reflect significant changes in particulate Hg with depth. For example, at 150 m the THg to bulk particulate carbon ratio (THg/PC) increases abruptly (Table S4a,b; Umhau et al., 2016), which is indicative of preferential organic carbon degradation (Close et al., 2014, 2015) or an increase in THg sorption that results in an enrichment of THg in particles. At this depth, $\delta^{202}Hg$ values of marine particles were more negative than surface samples, which suggests that the particulate increase in THg relative to PC is due to THg sorption to POM (Figure 2a; Jiskra et al., 2012; Wiederhold et al., 2010). At greater depths (400–690 m), $\delta^{202}Hg$ values show seasonal differences that are likely driven by temporal changes in marine particle export at Station ALOHA (Umhau et al., 2016). Samples collected in May coincided with the beginning of a period of increased productivity, while samples collected in September coincided with the middle to end of the commonly observed seasonal bloom at ALOHA, which is marked by higher concentrations of PC and bulk nitrogen across small and large particle size classes and high particle export fluxes (Church et al., 2013; Umhau et al., 2016). The increase in $\delta^{202}Hg$ values of particles sampled at 400–690 m in May and September (Figure 2a) likely reflects this period of increased productivity at Station ALOHA (Church et al., 2013; Umhau et al., 2016). This interpretation agrees with the findings of Hannides et al. (2016), who provided evidence for increased microbial reworking of small particles in September and May relative to zooplankton grazing.

4.3. Methylation of Hg in the Water Column

The THg isotopic composition of marine particles serves as a marker of the Hg available for methylation and subsequent bioaccumulation, and as such, it can also be used as a proxy for examining Hg methylation. The specific mechanism for methylation of Hg (II) in the open ocean water column is uncertain but is likely microbially mediated, as it is in freshwater and terrestrial ecosystems (Cossa et al., 2009, 1997; Morel et al., 1998; Sunderland et al., 2009). There is, however, also evidence from filtered seawater experiments (Munson et al., 2018) for noncellular or extracellular methylation in the water column in the oligotrophic Pacific. Methylation of Hg in the water column was also shown to be consistent with patterns of Hg isotope variation with the depth of marine fish feeding (Blum et al., 2013). Here, we use measured particle THg concentrations and isotopic compositions to infer the isotopic composition of MMHg available for consumption. Although we lack direct measurements of particle MMHg abundance and isotopic composition, previous experimental work has shown that the MMHg produced has lower $\delta^{202}Hg$ values compared to that of reactant Hg (II) (Janssen et al., 2016; Rodriguez-Gonzalez et al., 2009). If the extent of methylation is high enough, residual Hg (II) will have detectably higher $\delta^{202}Hg$ than reactant Hg (II). Experimental studies have also demonstrated that methylation of Hg by microbial processes results in MDF but not MIF (Janssen et al., 2016; Rodriguez-Gonzalez et al., 2009).

In order to aid in the interpretation of Hg isotope measurements made in this study, within the context of Hg methylation in the water column, we have listed five assumptions that we have made based on previous research on the biological pump and Hg stable isotope behavior:

1. The difference in $\delta^{202}Hg$ values between precipitation and particles in surface waters results from MDF of Hg (II) during sorption to particles (Jiskra et al., 2012; Wiederhold et al., 2010) and equilibration with the existing pool of Hg (II) in the surface ocean.
2. The main zone of particle production at Station ALOHA is within the mixed layer, and maximum particle remineralization occurs immediately below the deep chlorophyll maximum (Figure S1; Benitez-Nelson et al., 2001; Steinberg et al., 2008), which in this study was at ~125 m.
3. In the mesopelagic zone, large particles (> 53 μm) are exploited as a food resource by zooplankton during all seasons, and small particles (1–53 μm) become an important source during the winter (Hannides et al., 2016).
4. MMHg accumulated in particles by methylation of Hg (II) is efficiently bioaccumulated by consumers and incorporated in the pelagic food web by zooplankton grazing. The Hg (II) that is not bioaccumulated is excreted as fecal pellets at depth (Mason et al., 1996) leading to a relative increase of Hg (II) in the large particles at depth. These large fecal pellets can also be modified by sloppy feeding from zooplankton (Steinberg & Landry, 2017) resulting in an increase of Hg (II) in the small particles at depth.

5. Photochemical degradation of MMHg in sunlit surface water results in elevated Δ^{199}Hg values. Since there are no known mechanisms in aquatic systems for erasing that MIF, except by dilution with newly formed MMHg at depths below the euphotic zone that does not have elevated Δ^{199}Hg values, observed decreases in Δ^{199}Hg (and δ^{202}Hg) values in marine organisms with depth requires Hg methylation below the euphotic zone (Blum et al., 2013; Cossa et al., 2009).

Evidence that newly methylated Hg carried by particles enters the pelagic marine food web is illustrated by the δ^{202}Hg values in Figure 2a. We observe significantly higher δ^{202}Hg values associated with particles collected in deeper waters (400–700 m, Figure 2a) relative to δ^{202}Hg values measured in particles from the upper 150 m around the period of the rapid particle export pulse below the mixed layer (150 m) typically observed at Station ALOHA (Böttjer et al., 2017; Karl et al., 2012). We propose that the increased productivity at these depths (Church et al., 2013; Hannides et al., 2016) may stimulate methylation of Hg resulting in an increase in δ^{202}Hg values at this depth between May and September. An increase in δ^{202}Hg values is supported by findings from microbial methylation experiments (Janssen et al., 2016; Rodriguez-Gonzalez et al., 2009) and the fact that below 150 m the concentration of particulate THg is similar regardless of the season (Figure S2), whereas the MMHg content has been observed to increase (Hammerschmidt & Bowman, 2012; Munson et al., 2014). For zooplankton and fish, lower δ^{202}Hg values are also observed with increasing depth (Figures 2a and S4a). This is consistent with zooplankton preferentially bioaccumulating MMHg and discarding Hg (II) in their fecal matter (Mason et al., 1996); the newly formed MMHg with lower δ^{202}Hg values deeper in the water column is preferentially assimilated leaving the residual particulate Hg (II) with increasingly higher δ^{202}Hg values. Residual Hg is continuously incorporated into the POM shifting its Hg isotopic composition to higher δ^{202}Hg values at depth. Our results are consistent with the argument by Blum et al. (2013) that the decreasing δ^{202}Hg and Δ^{199}Hg values in predatory fish provides evidence that new MMHg formed at depth is incorporated into the food web.

While Δ^{199}Hg values of pelagic fish decrease with depth (indicating Hg methylation), the Δ^{199}Hg values of zooplankton collected at and below the chlorophyll maximum display minimal variation with depth or time of day (Figures 2b and S4b). We suggest that the invariant Δ^{199}Hg values of zooplankton with depth are a result of diurnal migration and MMHg demethylation (see section 4.4.2). Zooplankton occupy an intermediate trophic position between marine particles and fish resulting in a mixture of Hg (II) and MMHg that may obscure any methylation or demethylation signal of Hg because both pools are represented in the THg isotope composition of the zooplankton, and they have complementary Δ^{199}Hg values. As such, the migration of zooplankton from greater depths to surface waters likely results in mixing of THg in the water column by predation and digestion. The mixed pool of Hg in the zooplankton and the continuous incorporation of surface material at depth, with Δ^{199}Hg values fractionated by photodegradation, obscures the relationship of Δ^{199}Hg and depth. An exception to constant Δ^{199}Hg values with depth is at 400 m for the intermediate and large zooplankton (Figures 2b and S3b), where the Δ^{199}Hg value from the intermediate and large-size zooplankton collected at night is higher than the value measured in the sample collected during the day. This Δ^{199}Hg diurnal variation coincides with greater δ^{202}Hg values during the day for the large zooplankton size fraction (Figures 2b and S4b). These diurnal isotope signatures at 400 m also coincide with elevated THg concentrations within the intermediate and large size fractions sampled at night (Figure 3b), and this is the depth interval where there is elevated migrant biomass of zooplankton (Hannides et al., 2016). This indicates that the Hg isotopic composition of zooplankton in this depth range is likely affected by diurnal migration, but it is unclear how it results in greater Δ^{199}Hg values. A more complete understanding of Hg in zooplankton is needed to fully evaluate the pathways affecting these Hg isotope signatures. It is important to note that the large size fraction also contains some small fish (e.g., *Cyclothone*), which may further complicate isotope patterns, as small fish are likely to migrate differently than zooplankton.

4.4. Demethylation of MMHg in the Water Column

Demethylation occurs by either photochemical degradation, which leaves residual MMHg in the reactant pool with higher Δ^{199}Hg values and higher δ^{202}Hg values (Bergquist & Blum, 2007), or by microbial degradation, which also results in higher δ^{202}Hg values for residual MMHg but does not change Δ^{199}Hg values (Kritee et al., 2009). Although photodemethylation is an important process, it only occurs in the upper euphotic zone where there is significant light penetration; microbial demethylation is expected to occur throughout the water column and is the dominant process that breaks down MMHg in deeper waters.

4.4.1. Photochemical Demethylation Within the Mixed Layer

In surface waters the photochemical degradation of MMHg is the dominant pathway for breakdown of MMHg to Hg (II) and Hg(0) (Mason et al., 2012), but the exact mechanism and rate controlling factors remain uncertain (Black et al., 2012; Hammerschmidt & Fitzgerald, 2006; Inoko, 1981; Lehnherr & St. Louis, 2009; Suda et al., 1993; Zhang & Hsu-Kim, 2010). Based on Hg stable isotope experimental and field data (Bergquist & Blum, 2007; Chandan et al., 2015), the $\Delta^{199}Hg/\Delta^{201}Hg$ ratio has been shown to be diagnostic of photochemical reactions of Hg mediated by a radical pair mechanism. For example, in experiments with natural organic matter, photoreduction of Hg (II) produced $\Delta^{199}Hg/\Delta^{201}Hg = 1.00$ and photoreduction of MMHg produced $\Delta^{199}Hg/\Delta^{201}Hg = 1.36$ (Bergquist & Blum, 2007). Other Hg (II) photoreduction experiments with cysteine and serine showed that the ratio of $\Delta^{199}Hg$ to $\Delta^{201}Hg$ values is sensitive to the binding ligand, reaction conditions, and specifically to radical pair intermediates (Zheng & Hintelmann, 2010). For Station ALOHA the $\Delta^{199}Hg/\Delta^{201}Hg$ ratio (Figure 4a) for all samples measured, with the exception of precipitation, was 1.21 ± 0.003 (York Regression, 1 SD). This slope from the NPSG samples is similar to other marine and estuary fish studies (1.23 ± 0.01, 1 SD; Gehrke et al., 2011; Kwon et al., 2015; Li et al., 2016; Sackett et al., 2017; Senn et al., 2010) suggesting that the MIF values were produced by similar MMHg photochemical degradation mechanisms. This is supported by the good correlation between $\Delta^{199}Hg$ and $\delta^{202}Hg$ with a slope of 2.68 ± 0.12 (Figure 4b, 1 SD), which agrees with the experimentally derived photochemical degradation slope for MMHg of 2.43 ± 0.10 (Bergquist & Blum, 2007). The $\Delta^{199}Hg$ values reported here can be used to examine the photodegradation of MMHg available for uptake at the base of the food web, but because we did not measure the Hg isotopic composition of dissolved MMHg, we are unable to fully characterize the isotopic signature for degradation of dissolved MMHg. Many pathways for the photodegradation of MMHg have been identified, but not all of these may represent the MMHg pool that is taken up by pelagic fish. For example, residual photodegraded MMHg associated with high molecular weight dissolved organic matter is not available for passive uptake by phytoplankton (see Figure 1; Gorski et al., 2006; Lee & Fisher, 2017; Mason et al., 1996) and it is likely not representative of the THg isotopic signatures of the small zooplankton, which feed on phytoplankton in surface waters (Lee & Fisher, 2016; Steinberg & Landry, 2017).

$\Delta^{199}Hg$ values presented here can be used to track the photochemical degradation of biologically active MMHg that enters the marine food web in surface waters. The high $\delta^{202}Hg$ and $\Delta^{199}Hg$ values measured in samples from each zooplankton size class and in fish from the shallowest waters at Station ALOHA are consistent with the accumulation of Hg that has been photochemically modified in surface waters (Figures 2a and 2b). The $\Delta^{199}Hg$ values of surface (25 m) zooplankton display a clear diurnal pattern, where $\Delta^{199}Hg$ values are greater during the day than at night, and their isotopic composition is significantly higher than deeper samples (125–1,250 m, Wilcoxon test, $W = 15$, $p < 0.01$). A diurnal cycle of $\Delta^{199}Hg$ values in zooplankton is expected given the recent reports that marine phytoplankton and bacterioplankton can photochemically degrade Hg (Grégoire & Poulain, 2016; Kritee et al., 2017; Lee & Fisher, 2018). We suggest the $\Delta^{199}Hg$ value in surface zooplankton represents the isotopic composition of photodegraded MMHg in phytoplankton or particle-associated MMHg that has been photodemethylated before entering the food web. Elevated $\Delta^{199}Hg$ values of small zooplankton relative to the other size fractions are attributed to a tight linkage between zooplankton (0.06–0.2 and 0.2–0.5 mm) and primary productivity in surface waters at Station ALOHA, because surface water small zooplankton (e.g., copepods) obtain most of their MMHg from an algal dietary source (Lee & Fisher, 2017). Larger zooplankton may also exploit large POM as a dietary source resulting in lower $\Delta^{199}Hg$ values (Figure 1; Hannides et al., 2016), because the $\Delta^{199}Hg$ values associated with POM are very low. There is also a possibility that $\Delta^{199}Hg$ values at the surface are altered by diel migration, where migrant zooplankton bring to the surface new Hg with low $\Delta^{199}Hg$ values during the night resulting in day/night variations at the surface. However, a simple mixing model demonstrates that migrant associated Hg contributions would need to be about 53–55% and 95% of the total Hg in large and intermediate zooplankton, respectively. Such large contributions are unlikely given that at Station ALOHA night biomass is only about 1.7 times higher than the zooplankton biomass that is measured during the day (Hannides et al., 2016; see SI and references therein for details).

4.4.2. Demethylation Below the Mixed Layer

Patterns in $\Delta^{199}Hg$ values with depth for marine particles and zooplankton (Figure 2b) are consistent with active dark demethylation of Hg below the mixed layer, which was also suggested by Munson et al. (2018) based on an experimental study in the Pacific Ocean. The $\Delta^{199}Hg$ values of THg within particles are

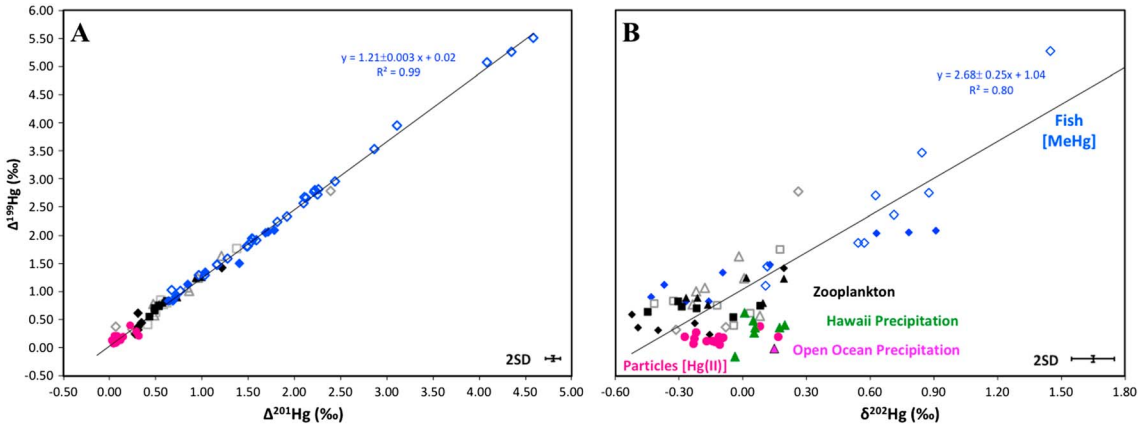

Figure 4. (a) Δ^{201}Hg versus Δ^{199}Hg and (b) δ^{202}Hg versus Δ^{199}Hg for samples analyzed in this study. The symbols and measurement uncertainty are the same as for Figures 2a and 2b.

relatively constant with depth as expected in the absence of light, with the exception of samples from 400 m and one sample from 690 m. At these depths the particles have significantly higher Δ^{199}Hg values (by 0.26‰ in February, 0.37‰ in September, and 0.18‰ in May) compared to all the samples collected at 25–150 m from all three seasons (average = 0.12 ± 0.05‰, 1 SD, n = 8). A possible explanation for the increase in Δ^{199}Hg values in marine particles with depth is demethylation of MMHg within the water column. MMHg is expected to have elevated Δ^{199}Hg values (relative to the Hg (II)) from photodecomposition, as indicated by the THg isotopic composition of pelagic fish, which usually contain >95% MMHg. This suggests that the Hg (II) newly formed from MMHg will have elevated Δ^{199}Hg values compared to the Hg (II) derived from precipitation, and we propose that this product Hg (II) may be incorporated into marine particles with depth.

There is incomplete understanding of the sources and sinks of Hg at depth, and this makes it difficult to specify with certainty a single mechanism for demethylation. Migrating zooplankton may also contribute to the increase in Δ^{199}Hg values within particles by adding fecal pellets with elevated THg. It has been shown that zooplankton primarily bioaccumulate MMHg and discard Hg (II) in their fecal pellets, which are an important source to POM below the twilight zone (Figure 1; Mason et al., 1996). However, demethylation of MMHg to Hg (II) within the water column is supported by the constant values for Δ^{199}Hg in zooplankton with depth (Figures 2b and S4b), since THg in zooplankton is a combination of MMHg and Hg (II), and the THg isotopic composition of zooplankton represents a weighted average of the two end members. The proportion of MMHg within zooplankton is expected to increase with depth, because dissolved MMHg and MMHg in pelagic fish has been shown to also increase with depth. The increasing MMHg concentrations with depth suggest that if only methylation and diel migration were altering the pool of Hg available to the food web, we would find lower values of Δ^{199}Hg with increasing depth in the zooplankton, as is the case with pelagic fish.

5. Conclusions

At Station ALOHA in the North Pacific Ocean, Hg stable isotope ratios and concentrations indicate that Hg from precipitation represents the major source of Hg to marine pelagic waters. After deposition, a portion of this Hg is sorbed to marine particles. This is supported by an overlap in Δ^{199}Hg values between precipitation and marine particles in surface waters and the consistent difference in δ^{202}Hg values between precipitation and particles, which we attribute to MDF accompanying sorption. The negative shift in δ^{202}Hg values in particles at 150 m compared to surface particles corresponds to a sharp increase in the ratio of THg to PC within marine particles (Umhau et al., 2016). Δ^{199}Hg values measured in particles between 400 and 700 m and the invariant Δ^{199}Hg values in zooplankton at various depths below the photic zone demonstrate that the production and degradation of MMHg occurs throughout the water column. The isotopic trends demonstrate a tight link in Hg uptake between particles and zooplankton and that the bioaccumulation of MMHg

depends on particle formation and degradation as well as the activity of zooplankton (both vertically migrating and resident) that mobilize and modify the THg content of sinking and suspended particles. The nearly constant $\Delta^{199}Hg/\Delta^{201}Hg$ ratios throughout the marine food web suggests that the pool of bioaccumulated MMHg is partially photochemically degraded by a process that includes radical pair formation and that is ubiquitous in marine ecosystems. Our results highlight the importance and impact that particles and zooplankton have in the marine biogeochemical cycle of Hg. Additional detailed studies of Hg isotope ratios in marine food webs are needed and should include seasonal studies as well as studies in nonoligotrophic environments. A more complete understanding of the mechanisms controlling Hg isotope variations in the pelagic ocean will allow better modeling of the biogeochemical cycle of Hg.

Acknowledgments
We thank S. Wakeham, E. DeLong, and K. Maiti for providing McLane pumps and T. Shanahan of McLane Research Laboratories for providing 30 L/min pump components. We also thank K. Miyano, A. Leitner, and C. Ka'apu-Lyons from the U. of Hawaii, who helped with sample collection and McLane pump and MOCNESS deployments. Finally, thanks to the captain and crew of the R/V *Kilo Moana* and the UH Ocean Technology Group. This work was supported by National Science Foundation (NSF) grants OCE 1433710 (to J. D. Blum), OCE 1333734 (to J. C. Drazen, H. G. Close, B. N. Popp, and C. C. S. Hannides), OCE 1433846 (to B. N. Popp, J. C. Drazen, and C. C. S. Hannides), and OCE 1433313 (to C. R. Benitez-Nelson) and an NSF Graduate Fellowship to L. Motta. This is SOEST contribution number 10716. All THg and Hg stable isotope data are available in the supporting information tables and in the website (https://www.bco-dmo.org/project/560580).

References

Andersson, M., Sommar, J., Gårdfeldt, K., & Jutterström, S. (2011). Air-sea exchange of volatile mercury in the North Atlantic Ocean. *Marine Chemistry*, *125*(1-4), 1–7. https://doi.org/10.1016/j.marchem.2011.01.005

Benitez-Nelson, C. R., Buesseler, K. O., Karl, D. M., & Andrews, J. E. (2001). A time-series study of particulate matter export in the North Pacific Subtropical Gyre based on ^{234}Th:^{238}U disequilibrium. *Deep-Sea Research Part I: Oceanographic Research Papers*, *48*(12), 2595–2611. https://doi.org/10.1016/S0967-0637(01)00032-2

Bergquist, B., & Blum, J. D. (2007). Mass-dependent and independent fractionation of Hg isotopes by photoreduction in aquatic systems. *Science*, *318*(5849), 417–420. https://doi.org/10.1126/science.1148050

Bishop, J. K. B., Lam, P. J., & Wood, T. J. (2012). Getting good particles: Accurate sampling of particles by large volume in-situ filtration. *Limnology and Oceanography: Methods*, *10*(9), 681–710. https://doi.org/10.4319/lom.2012.10.681

Biswas, A., Blum, J. D., Bergquist, B. A., Keeler, G. J., & Xie, Z. (2008). Natural mercury isotope variation in coal deposits and organic soils. *Environmental Science and Technology*, *42*(22), 8303–8309. https://doi.org/10.1021/es801444b

Black, F. J., Poulin, B. A., & Flegal, A. R. (2012). Factors controlling the abiotic photo-degradation of monomethylmercury in surface waters. *Geochimica et Cosmochimica Acta*, *84*, 492–507. https://doi.org/10.1016/j.gca.2012.01.019

Blum, J. D., & Bergquist, B. A. (2007). Reporting of variations in the natural isotopic composition of mercury. *Analytical and Bioanalytical Chemistry*, *388*(2), 353–359. https://doi.org/10.1007/s00216-007-1236-9

Blum, J. D., & Johnson, M. W. (2017). Recent developments in mercury stable isotope analysis. Non-traditional isotope geochemistry. *Reviews in Mineralogy and Geochemistry*, *82*(1), 733–757. https://doi.org/10.2138/rmg.2017.82.17

Blum, J. D., Popp, B. N., Drazen, J. C., Choy, C. A., & Johnson, M. W. (2013). Methylmercury production below the mixed layer in the North Pacific Ocean. *Nature Geoscience*, *6*(10), 879–884. https://doi.org/10.1038/ngeo1918

Blum, J. D., Sherman, L. S., & Johnson, M. W. (2014). Mercury isotopes in Earth and environmental science. *Annual Review of Earth and Planetary Sciences*, *42*(1), 249–269. https://doi.org/10.1146/annurev-earth-050212-124107

Böttjer, D., Dore, J. E., Karl, D. M., Letelier, R. M., Mahaffey, C., Wilson, S. T., et al. (2017). Temporal variability of nitrogen fixation and particulate nitrogen export at Station ALOHA. *Limnology and Oceanography*, *62*(1), 200–216. https://doi.org/10.1002/lno.10386

Chandan, P., Ghosh, S., & Bergquist, B. A. (2015). Mercury isotope fractionation during aqueous photoreduction of monomethylmercury in the presence of dissolved organic matter. *Environmental Science and Technology*, *49*(1), 259–267. https://doi.org/10.1021/es5034553

Chen, J., Hintelmann, H., Feng, X., & Dimock, B. (2012). Unusual fractionation of both odd and even mercury isotopes in precipitation from Peterborough, ON, Canada. *Geochimica et Cosmochimica Acta*, *90*, 33–46. https://doi.org/10.1016/j.gca.2012.05.005

Choy, C. A., Popp, B. N., Hannides, C. C. S., & Drazen, J. C. (2015). Trophic structure and food resources of epipelagic and mesopelagic fishes in the North Pacific Subtropical Gyre ecosystem inferred from nitrogen isotopic compositions. *Limnology and Oceanography*, *60*(4), 1156–1171. https://doi.org/10.1002/lno.10085

Choy, C. A., Popp, B. N., Kaneko, J. J., & Drazen, J. C. (2009). The influence of depth on mercury levels in pelagic fishes and their prey. *Proceedings of the National Academy of Sciences of the United States of America*, *106*(33), 13,865–13,869. https://doi.org/10.1073/pnas.0900711106

Church, M. J., Lomas, M. W., & Muller-karger, F. (2013). Deep-sea research II sea change: Charting the course for biogeochemical ocean time-series research in a new millennium. *Deep-Sea Research Part II: Topical Studies in Oceanography*, *93*, 2–15. https://doi.org/10.1016/j.dsr2.2013.01.035

Close, H. G., Hannides, C. S., Drazen, J. C., & Popp, B. N. (2015). Degradative transformations of stable isotope ratios in sinking and suspended organic matter, from surface to upper bathypelagic depths, Station ALOHA. 2015 Aquatic Sciences Meeting (Granada, Spain).

Close, H. G., Hannides, C. S., & Popp, B. N. (2014). Compound-specific values as indicator of biosynthesis and degradation in marine particles, from submicron to sinking at Station ALOHA. 2014 Ocean Sciences Meeting (Honolulu, HI).

Cossa, D., Averty, B., & Pirrone, N. (2009). The origin of methylmercury in open Mediterranean waters. *Limnology and Oceanography*, *54*(3), 837–844. https://doi.org/10.4319/lo.2009.54.3.0837

Cossa, D., Heimbürger, L. E., Lannuzel, D., Rintoul, S. R., Bultler, E. C. V., Bowie, A. R., et al. (2011). Mercury in the Southern Ocean. *Geochimca et Cosmochimca Acta*, *75*(14), 4037–4052. https://doi.org/10.1016/j.gca.2011.05.001

Cossa, D., Heimbürger, L. E., Sonke, J. E., Planquette, H., Lherminier, P., García-Ibáñez, M. I., et al. (2018). Sources, cycling and transfer of mercury in the Labrador Sea (Geotraces-Geovide cruise). *Marine Chemistry*, *198*, 64–69. https://doi.org/10.1016/j.marchem.2017.11.006

Cossa, D., Martin, J.-M., Takayanagi, K., & Sanjuan, J. (1997). The distribution and cycling of mercury species in the western Mediterranean. *Deep-Sea Research Part II: Topical Studies in Oceanography*, *44*(3-4), 721–740. https://doi.org/10.1016/S0967-0645(96)00097-5

Demers, J. D., Blum, J. D., & Zak, D. R. (2013). Mercury isotopes in a forested ecosystem: Implications for air-surface exchange dynamics and the global mercury cycle. *Global Biogeochemical Cycles*, *27*, 222–238. https://doi.org/10.1002/gbc.20021

Fisher, J. A., Jacob, D. J., Soerensen, A. L., Amos, H. M., Steffen, A., & Sunderland, E. M. (2012). Riverine source of Artic Ocean mercury inferred from atmospheric observations. *Nature Geoscience*, *5*(7), 499–504. https://doi.org/10.1038/ngeo1478

Fitzgerald, W. F., Lamborg, C. H., & Hammerschmidt, C. R. (2007). Marine biogeochemical cycling of mercury. *Chemical Reviews*, *107*(2), 641–662. https://doi.org/10.1021/cr050353m

Gehrke, G. E., Blum, J. D., & Marvin-DePasquale, M. (2011). Sources of mercury to San Francisco Bay surface sediment as revealed by mercury stable isotopes. *Geochimica et Cosmochimca Acta*, *75*(3), 691–705. https://doi.org/10.1016/j.gca.2010.11.012

Gloeckler, K., Choy, C. A., Hannides, C. C., Close, H. G., Goetze, E., Popp, B. N., & Drazen, J. C. (2018). Stable isotope analysis of micronekton around Hawaii reveals suspended particles are an important nutritional source in the lower mesopelagic and upper bathypelagic zones. *Limnology and Oceanography*, *63*(3), 1168–1180. https://doi.org/10.1002/lno.10762

Gorski, P. R., Armstrong, D. E., Hurley, J. P., & Shafer, M. M. (2006). Speciation of aqueous methylmercury influences uptake by freshwater alga (Selenastrum capricornutum). *Environmental Toxicology and Chemistry*, *25*(2), 534–540. https://doi.org/10.1897/04-530R.1

Gosnell, K. J., & Mason, R. P. (2015). Mercury and methylmercury incidence and bioaccumulation in plankton from the central Pacific Ocean. *Marine Chemistry*, *177*, 772–780. https://doi.org/10.1016/j.marchem.2015.07.005

Gratz, L. E., Keeler, G. J., Blum, J. D., & Sherman, L. S. (2010). Isotopic composition and fractionation of mercury in Great Lakes precipitation and ambient air. *Environmental Science and Technology*, *44*(20), 7764–7770. https://doi.org/10.1021/es100383w

Grégoire, D. S., & Poulain, A. J. (2016). A physiological role for HgII during phototrophic growth. *Nature Geoscience*, *9*(2), 121–125. https://doi.org/10.1038/ngeo2629

Hammerschmidt, C. R., & Bowman, K. L. (2012). Vertical methylmercury distributions in the subtropical North Pacific Ocean. *Marine Chemistry*, *132–133*, 77–82.

Hammerschmidt, C. R., Finiguerra, M. B., Weller, R. L., & Fitzgerald, W. F. (2013). Methylmercury accumulation in plankton on the continental margin of the northwest Atlantic Ocean. *Environmental Science and Technology*, *47*(8), 3671–3677. https://doi.org/10.1021/es3048619

Hammerschmidt, C. R., & Fitzgerald, W. F. (2006). Methylmercury cycling in sediments on the continental shelf of southern New England. *Geochimica et Cosmochimca Acta*, *70*(4), 918–930. https://doi.org/10.1016/j.gca.2005.10.020

Hannides, C. C., Popp, B. N., Close, H. G., Benitez-Nelson, C. R., Ka'apu-Lyons, C. A., Gloecker, K., et al. (2016). Midwater zooplankton response to seasonality in export flux in the North Pacific Subtropical Gyre. 2016 Ocean Sciences Meeting (New Orleans, LA).

Hedgecock, I. M., & Pirrone, N. (2001). Mercury and photochemistry in the marine boundary layer-modelling studies suggest the in situ production of reactive gas phase mercury. *Atmospheric Environment*, *35*(17), 3055–3062. https://doi.org/10.1016/s1352-2310(01)00109-1

Inoko, M. (1981). Studies on the photochemical decomposition of organomercurials–methylmercury (II) chloride. *Environmental Pollution*, *B2*, 3–10.

Janssen, S. E., Schaefer, J. K., Barkay, T., & Reinfelder, J. R. (2016). Fractionation of mercury stable isotopes during microbial methylmercury production by iron- and sulfate-reducing bacteria. *Environmental Science and Technology*, *50*, 8077–8083. https://doi.org/10.1021/acs.est.6b00854

Jiskra, M., Wiederhold, J. G., Bourdon, B., & Kretzschmar, R. (2012). Solution speciation controls mercury isotope fractionation of Hg (II) sorption to goethite. *Environmental Science and Technology*, *46*(12), 6654–6662. https://doi.org/10.1021/es3008112

Karl, D. M., Church, M. J., Dore, J. E., Letelier, R. M., & Mahaffey, C. (2012). Predictable and efficient carbon sequestration in the North Pacific Ocean supported by symbiotic nitrogen fixation. *Proceedings of the National Academy of Sciences of the United States of America*, *109*(6), 1842–1849. https://doi.org/10.1073/pnas.1120312109

Kritee, K., Barkay, T., & Blum, J. D. (2009). Mass dependent stable isotope fractionation of mercury during mer mediated microbial degradation of monomethylmercury. *Geochimica et Cosmochimica Acta*, *73*(5), 1285–1296. https://doi.org/10.1016/j.gca.2008.11.038

Kritee, K., Motta, L. C., Blum, J. D., Tsui, M. T., & Reinfelder, J. R. (2017). Photomicrobial visible light-induced magnetic mass independent fractionation of mercury in marine microalga. *Earth and Space Chemistry*, *2*, 432–440.

Kwon, S. Y., Blum, J. D., Chen, C. Y., Meattey, D. E., & Mason, R. P. (2015). Mercury isotope study of sources and exposure pathways of methylmercury in estuarine food webs in the Northeastern US. *Environmental Science and Technology*, *48*, 10,089–10,097.

Lamborg, C. H., Hammerschmidt, C. R., & Bowman, K. L. (2016). An examination of the role of particles in oceanic mercury cycling. *Philosophical Transactions of the Royal Society A*, *374*(2081), 20150297. https://doi.org/10.1098/rsta.2015.0297

Lamborg, C. H., Hammerschmidt, C. R., R, C., Gill, G. A., Mason, R. P., & Gichuki, S. (2012). An intercomparison of procedures for the determination of total mercury in seawater and recommendations regarding mercury speciation during GEOTRACES cruises. *Limnology and Oceanography: Methods*, *10*(2), 90–100. https://doi.org/10.4319/lom.2012.10.90

Lamborg, C. H., von Damm, K. L., Fitzgerald, W. F., Hammerschmidt, C. R., & Zierenberg, R. (2006). Mercury and monomethylmercury in fluids from Sea Cliff submarine. *Geophysical Research Letters*, *33*, L17606. https://doi.org/10.1029/2006GL026321

Lamborg, C. H., Tseng, C.-M., Fitzgerald, W. F., Balcom, P. H., & Hammerschmidt, C. R. (2003). Determination of the Mercury Complexation Characteristics of Dissolved Organic Matter in Natural Waters with « Reducible Hg » Titrations. *Environmental Science & Technology*, *37*(15), 3316–3322. https://doi.org/10.1021/es0264394

Landis, M. S., & Keeler, G. J. (1997). Critical evaluation of a modified automatic wet-only precipitation collector for mercury and trace element determinations. *Environmental Science and Technology*, *31*(9), 2610–2615. https://doi.org/10.1021/es9700055

Lauretta, D. S., Klaue, B., Blum, J. D., & Buseck, P. R. (2001). Mercury abundances and isotopic compositions in the Murchison (CM) and Allende (CV) carbonaceous chondrites. *Geochimica et Cosmochimca Acta*, *65*(16), 2807–2818. https://doi.org/10.1016/S0016-7037(01)00630-5

Laurier, F. J. G., Mason, R. P., Gill, G. A., & Whalin, L. (2004). Mercury distributions in the North Pacific Ocean—20 years of observations. *Marine Chemistry*, *90*(1-4), 3–19. https://doi.org/10.1016/j.marchem.2004.02.025

Lee, C. S., & Fisher, N. S. (2016). Methylmercury uptake by diverse marine phytoplankton. *Limnology and Oceanography*, *61*(5), 1626–1639. https://doi.org/10.1002/lno.10318

Lee, C. S., & Fisher, N. S. (2017). Bioaccumulation of methylmercury in a marine copepod. *Environmental Toxicology and Chemistry*, *36*(5), 1287–1293. https://doi.org/10.1002/etc.3660

Lee, C. S., & Fisher, N. S. (2018). Microbial generation of elemental mercury form dissolved methylmercury in seawater. *Limnology and Oceanography*, *00*, 1–15.

Lehnherr, I., & St. Louis, V. L. (2009). Importance of ultraviolet radiation in the photodemethylation of methylmercury in freshwater ecosystems. *Environmental Science and Technology*, *43*(15), 5692–5698. https://doi.org/10.1021/es9002923

Li, M., Schartup, A. T., Valberg, A. P., Ewald, J. D., Krabbenhoft, D. P., Yin, R., et al. (2016). Environmental origins of methylmercury accumulated in subarctic estuarine fish indicated by mercury stable isotopes. *Environmental Science and Technology*, *50*(21), 11,559–11,568. https://doi.org/10.1021/acs.est.6b03206

Mason, R. P., Choi, A. L., Fitzgerald, W. F., Hammerschmidt, C. R., Lamborg, C. H., Soerensen, A. L., & Sunderland, E. M. (2012). Mercury biogeochemical cycling in the ocean and policy implications. *Environmental Research*, *119*, 101–117. https://doi.org/10.1016/j.envres.2012.03.013

Mason, R. P., Reinfelder, J. R., & Morel, F. M. M. (1995). Bioaccumulation of mercury and methylmercury. *Water, Air, and Soil Pollution*, *80*(1-4), 915–921. https://doi.org/10.1007/BF01189744

Mason, R. P., Reinfelder, J. R., & Morel, F. M. M. (1996). uptake, toxicity, and trophic transfer of mercury in a coastal diatom. *Environmental Science and Technology*, *30*(6), 1835–1845. https://doi.org/10.1021/es950373d

Mason, R. P., & Sheu, G. (2002). Role of the ocean in the global mercury cycle. *Global Biogeochemical Cycles*, *16*(4), 1093. https://doi.org/10.1029/2001GB001440

Monperrus, M., Martin-Doimeadios, R. C. R., Scancar, J., Amouroux, D., Donard, O. F. X., & Adour, D. (2003). Simultaneous sample preparation and species-specific isotope dilution mass spectrometry analysis of monomethylmercury and tributyltin in a certified oyster tissue. *Analytical Chemistry*, *75*(16), 4095–4102. https://doi.org/10.1021/ac0263871

Morel, F. M. M., Kraepiel, A. M. L., & Amyot, M. (1998). The chemical cycle and bioaccumulation. *Annual Review of Ecology, Evolution, and Systematics*, *29*(1), 543–566. https://doi.org/10.1146/annurev.ecolsys.29.1.543

Munson, K. M., Babi, D., & Lamborg, C. H. (2014). Monomethylmercury determination from seawater using ascorbic-acid assisted direct ethylation. *Limnology and Oceanography: Methods*, *12*(1), 1–9. https://doi.org/10.4319/lom.2014.12.1

Munson, K. M., Lamborg, C. H., Boiteau, R. M., & Saito, M. A. (2018). Dynamic mercury methylation and demethylation in oligotrophic marine water. *Biogeosciences Discussions*, *15*(21), 6451–6460. https://doi.org/10.5194/bg-15-6451-2018

Munson, K. M., Lamborg, C. H., Swarr, G. J., & Saito, M. A. (2015). Mercury species concentrations and fluxes in the central tropical Pacific Ocean. *Global Biogeochemical Cycles*, *29*, 656–676. https://doi.org/10.1002/2015GB005120

Noble, A. E., Lamborg, C. H., Ohnemus, D. C., Lam, P. P., Goepfert, T. J., Measures, C. I., et al. (2012). Basin-scale plumes of cobalt, iron, and manganese emanating from the Benguela-Angola front in the South Atlantic Ocean. *Limnology and Oceanography*, *57*(4), 989–1010. https://doi.org/10.4319/lo.2012.57.4.0989

Pasulka, A. L., Landry, M. R., Taniguchi, D. A. A., Taylor, A. G., & Church, M. J. (2013). Temporal dynamics of phytoplankton and heterotrophic protists at Station ALOHA. *Deep-Sea Research Part II: Topical Studies in Oceanography*, *93*, 44–57. https://doi.org/10.1016/j.dsr2.2013.01.007

Rodriguez-Gonzalez, P., Epov, V. N., Bridou, R., Tessier, E., Guyoneaud, R., Monperrus, M., & Amouroux, D. (2009). Species specific stable isotope fractionation of mercury during Hg (II) methylation by an anaerobic bacteria (*Desulfobulbus propionicus*) under dark conditions. *Environmental Science & Technology*, *43*(24), 9183–9188. https://doi.org/10.1021/es902206j

Sackett, D. K., Drazen, J. C., Popp, B. N., Choy, C. A., Blum, J. D., & Johnson, M. W. (2017). Carbon, nitrogen, and mercury isotope evidence for the biogeochemical history of mercury in Hawaiian marine bottomfish. *Environmental Science & Technology*, *51*(23), 13,976–13,984. https://doi.org/10.1021/acs.est.7b04893

Senn, D. B., Chesney, E. J., Blum, J. D., Bank M.S., Maage, A., & Shine, J. P. (2010). Stable isotope (N, C, Hg) study of methylmercury sources and trophic transfer in the northern Gulf of Mexico. *Environmental Science and Technology*, *44*(5), 1630–1637. https://doi.org/10.1021/es902361j

Sprovieri, F., Hedgecock, I. M., & Pirrone, N. (2010). An investigation of the origins of reactive gaseous mercury in the Mediterranean marine boundary layer. *Atmospheric Chemistry and Physics*, *10*(8), 3985–3997. https://doi.org/10.5194/acp-10-3985-2010

Steinberg, D. K., & Landry, M. R. (2017). Zooplankton and the ocean carbon cycle. *Annual Review of Marine Science*, *9*(1), 413–444. https://doi.org/10.1146/annurev-marine-010814-015924

Steinberg, D. K., van Mooy, B. A. S., Buesseler, K. O., Boyd, P. W., Kobari, T., & Karl, D. M. (2008). Microbial vs. zooplankton control of sinking particle flux in the ocean's twilight zone. *Limnology and Oceanography*, *53*(4), 1327–1338. https://doi.org/10.4319/lo.2008.53.4.1327

Strode, S., Jaegle, L., Selin, N., Jacob, D., Park, R., Yantosca, R., et al. (2007). Air-sea exchange in the global mercury cycle. *Global Biogeochemical Cycles*, *21*, GB1017. https://doi.org/10.1029/2006GB002766

Štrok, M., Baya, P. A., & Hintelmann, H. (2015). The mercury isotope composition of Artic coastal seawater. *Comptes Rendus Geoscience*, *347*(7-8), 368–376. https://doi.org/10.1016/j.crte.2015.04.001

Suda, I., Suda, M., & Hirayama, K. (1993). Degradation of methyl and ethyl mercury by singlet oxygen generated from sea water exposed to sunlight or ultraviolet light. *Archives of Toxicology*, *67*(5), 365–368. https://doi.org/10.1007/BF01973709

Sunderland, E. M., Krabbenhoft, D. P., Moreau, J. W., Strode, S. A., & Landing, W. M. (2009). Mercury sources, distribution, and bioavailability in the North Pacific Ocean: Insights from data and models. *Global Biogeochemical Cycles*, *23*, GB2010. https://doi.org/10.1029/2008GB003425

Sunderland, E. M., & Mason, R. P. (2007). Human impacts on open ocean mercury concentrations. *Global Biogeochemical Cycles*, *21*, GB4022. https://doi.org/10.1029/2006GB002876

Umhau, B., Motta, L. C., Benitez-Nelson, C. R., Close, H. G., Hannides, C. C. S., Popp, B. N., et al. (2016). Characterization of mercury particle flux using 238U:234Th disequilibria in the North Pacific Subtropical Gyre. 2016 Ocean Sciences Meeting (New Orleans, LA).

Washburn, S. J., Blum, J. D., Demers, J. D., Kurz, A. Y., & Landis, R. C. (2017). Isotopic characterization of mercury downstream of historic industrial contamination in the South River, Virginia. *Environmental Science and Technology*, *51*(19), 10,965–10,973. https://doi.org/10.1021/acs.est.7b02577

Watras, C., & Bloom, N. (1992). Mercury and methylmercury in individual implications for bioaccumulation zooplankton. *Limnology and Oceanography*, *37*(6), 1313–1318. https://doi.org/10.4319/lo.1992.37.6.1313

Wiebe, P. H., Morton, A. W., Bradley, A. M., Backus, R. H., Craddock, J. E., Barber, V., et al. (1985). New developments in the MOCNESS, an apparatus for sampling zooplankton and micronekton. *Marine Biology*, *87*(3), 313–323. https://doi.org/10.1007/BF00397811

Wiederhold, J. G., Cramer, C. J., Daniel, K., Infante, I., Bourdon, B., & Kretzschmar, R. (2010). Equilibrium mercury isotope fractionation between dissolved Hg (II) species and thiol-bound Hg. *Environmental Science & Technology*, *44*(11), 4191–4197. https://doi.org/10.1021/es100205t

York, D. (1969). Least squares fitting of a straight line with correlated errors. *Earth and Planetary Science Letters*, *5*, 320–324.

Zaferani, S., Pérez-Rodríguez, M., & Biester, H. (2018). Diatom ooze—A large marine mercury sink. *Science*, *361*(6404), 797–800. https://doi.org/10.1126/science.aat2735

Zhang, T., & Hsu-Kim, H. (2010). Photolytic degradation of methylmercury enhanced by binding to natural organic ligands. *Nature Geoscience*, *3*(7), 473–476. https://doi.org/10.1038/ngeo892

Zheng, W., & Hintelmann, H. (2010). Isotope fractionation of mercury during Its photochemical reduction by low-molecular-weight organic compounds. *The Journal of Physical Chemistry. A*, *114*(12), 4246–4253. https://doi.org/10.1021/jp9111348

References From the Supporting Information

Heimbürger, L.-E., Cossa, D., Marty, J.-C., Migon, C., Averty, B., Dufour, A., & Ras, J. (2010). Methyl mercury distributions in relation to the presence of nano and picophytoplankton in an oceanic water column (Ligurian Sea, North-western Mediterranean). *Geochimica et Cosmochimica Acta*, *74*(19), 5549–5559. https://doi.org/10.1016/j.gca.2010.06.036

McGowan, J. A., & Walker, P. W. (1979). Structure in the copepod community of the North Pacific central gyre. *Ecological Monographs*, *49*(2), 195–226. https://doi.org/10.2307/1942513

Monperrus, M., Tessier, E., Amouroux, D., Leynaert, A., Huonnic, P., & Donard, O. F. X. (2007). Mercury methylation, demethylation and reduction rates in coastal and marine surface waters of the Mediterranean Sea. *Marine Chemistry*, *107*(1), 49–63. https://doi.org/10.1016/j.marchem.2007.01.018

Talley, L. (1993). Distribution and formation of North Pacific Intermediate Water. *Journal of Physical Oceanography*, *23*(3), 517–537. https://doi.org/10.1175/1520-0485(1993)023<0517:DAFONP>2.0.CO;2

Ueno, H., & Yasuda, I. (2003). Intermediate water circulation in the North Pacific subarctic and northern subtropical regions. *Journal of Geophysical Research*, *08*(C11), 3348. https://doi.org/10.1029/2002JC001372